LA-UR -90-3603

LA-UR--90-3603

DE91 001861

Los Alamos National Laboratory is operated by the University of California for the United States Department of Energy under contract W-7405-ENG-36.

TITLE: THREE DIMENSIONAL TRANSPORT BENCHMARK EXERCISE USING THREEDANT

AUTHOR(S): R. E. Alcouffe

SUBMITTED TO: Specialist's Meeting on Three-Dimensional Neutron Transport Benchmarks, 22-23 October 1990

DISCLAIMER

Los Alamos Los Alamos National Laboratory
Los Alamos, New Mexico 87545

FORM NO. 836 R4
ST. NO. 2629 5/81

Three Dimensional Transport Benchmark Exercise Using THREEDANT

by

R.E. Alcouffe
MS b226
Los Alamos National Laboratory
Los Alamos NM 87545
USA

I. Introduction.

As part of the effort to assess the ability to perform three dimensional transport calculations to solve problems in reactor physics, we describe the THREEDANT code and its application to the set of three-dimensional benchmark problems proposed by Prof. T. Takeda. As part of this benchmarking activity, we display some key indicators as to computational performance and efficiency while displaying the sensitivity of the eigenvalue to Sn order and to spatial mesh size in each of the problems. In order to understand what is being displayed, we summarize the solution strategy incorporated in the code.

THREEDANT is the three-dimensional follow-on to the ONEDANT-TWODANT[1] system which comprises an input, solver, and edit module. Thus in using the same input and edit modules for THREEDANT, we maintain the same format for problem input and edits as in the one- and two-dimensional codes. The solver portion of the three-dimensional code is also based upon the same solution strategy as the lower dimensional solvers. That is, we solve the neutral particle Boltzmann equation by von Neumann or source iteration. The discretization is multigroup in energy, Sn discrete ordinate in angle, and diamond difference with set-to-zero fixup in the spatial variables. The geometries and symmetries that can be represented are orthogonal XYZ and RZΘ on a rectangular mesh. Also arbitrary anisotropic scattering is allowed using a spherical harmonics expansion of the scattering source. The source iteration convergence is accelerated by a three-dimensional DSA method for both the inner and outer iterations. The inner iterations are on the within-group scattering source and the outer iterations are on the fission and upscatter sources. Any eigenvalue iterations are performed by the power method on the multigroup DSA equations accelerated by a Chebychev technique. The DSA equation itself is based upon a diffusion correction scheme with a seven point representation of the diffusion operator at the mesh vertices.

Thus the computational technique incorporated in the code involves inverting the transport operator given the source and then using the DSA method to update the source for both the inner and outer iterations and to compute the eigenvalue if required. Because of the discrete ordinates method applied to the first order form of the Boltzmann equation, the inversion of the transport operator is easily ordered as a lower triangular matrix operation. Thus the inversion is accomplished by sweeping the mesh for each angle in a non-iterative manner. On vector computers

the sweeping can be vectorized by solving on mesh diagonals in a plane where solution and possible fixups can be computed simultaneously. In THREEDANT we have chosen the XY or RZ planes as the planes of vectorized solution which puts a bias in the efficiency of solution on these planes. This is illustrated in the benchmark problems where we have refined the mesh in the chosen XY plane and notice an increase in efficiency of solution indicated by a decrease in the average CPU time per phase space cell, T.

The seven point DSA equation is inverted using a three-dimensional multigrid technique. A multigrid cycle consists in relaxing the solution on a fine grid, transferring the residual and the diffusion operator to a coarser grid, relaxing on that grid to obtain a correction solution for the finer grid, and repeating the procedure until a coarsest grid is attained. The correction solution on the coarsest grid is obtained by a direct inversion of the diffusion operator. The correction is then interpolated onto the finer grids and added to the correction solution previously obtained there until the finest grid is attained. This cycle of computations usually reduces the error in the diffusion by an order of magnitude and thus is highly efficacious. Thus the main operations for the multigrid method is the relaxation method, the interpolation method and the residual and operator transference. In THREEDANT, we use line relaxation in each of the coordinate directions, we use linear interpolation based upon continuity of the diffusion current, and the transference of residuals is the transpose of the interpolation. The transference of the diffusion operator is based upon a simplified homogenization procedure in order to preserve the seven point character of the matrix representation on all grids. All of these processes are vectorizable and a good amount of effort has been made to ensure that the three-dimensional multigrid algorithm is vectorized. In the problem results, we include the equivalent number of fine grid relaxation sweeps required for the entire plus the average CPU time/mesh cell for an average work unit which is the time for an entire mesh sweep using line relaxation. The effect of vectorization is seen by the decrease in this time as the number of mesh cells increase.

II. Computational Performance.

We here make some comments on the data presented in the results section of this report on each of the benchmark problems computed in this exercise. The problems we solve are the LWR configuration given in Fig. 1 and the two FBR systems representable in XYZ geometry as shown in Figs. 2 and 3. In each problem we present the k eigenvalue of the system for each of the cases as a function of Sn order going from S-4 (3 angles per octant) to S-16 (36 angles per octant). We see from the results that the eigenvalue is well converged in Sn order by S-8 for the LWR and the larger FBR. The small FBR is converged to one part in 1.0e-5 by S-8 when the control rod is half inserted. We also give an indication of the dependency of k on spatial mesh refinement by presenting results with the number of mesh intervals in the XY plane doubled in each coordinate direction. For the FBR systems, this effect is larger than the Sn dependency yet the problems seem well converged spatially.

The second item we present is the computational time devoted to solving the problems as a function of Sn order and case. The results are broken down into the time devoted to the transport

space-angle sweeping and the DSA solution. The times are quoted in units of Cray YMP/8128 CPU seconds with some indication of time also in XMP/24 CPU seconds. What is clear from all of the problems is that the DSA time is about constant as a function of Sn order as would be hoped. Also the time devoted to the DSA is about twice that of performing the transport sweeps in S-4 and about 1.5 time less in S-8. Thus for the common Sn orders used to solve reactor physics problems, the time spent in solving the DSA equations is an important fraction of the total time, and thus it is very beneficial to reduce this time.

Thirdly, we indicate the performance of the iteration strategy by displaying the number of iterations to achieve the solution to an tolerance of 5.0e-5 in both the transport and diffusion stages. The iteration strategy employed in the code is to perform one transport sweep per group per outer iteration until the fission source is converged to the specified tolerance. Then the inner iterations are allowed to converge to obtain the final transport solution for the flux. The diffusion outers are the number of multigroup diffusion iterations required to converge the fission source; these have sometimes been referred to as sub-outers of the whole transport iteration process involved in DSA. The transport inner number is the total number of transport sweeps through the space-angle mesh in order to achieve the solution. Finally, the diffusion inners is the total number of line relaxation sweeps through the spatial mesh in one coordinate direction in the process of inverting the diffusion operator. The results presented are for the S-8 reference cases and show results which are comparable to two-dimensional cases. Thus it is apparent that the DSA is effective in accelerating convergence for these problems and thus the method is computationally efficient.

The last entry gives the CPU time on a per cell basis for the transport and diffusion sweeps in the reference discretization and the spatially refined discretization. It is seen that as the number of mesh cells increases, the time per cell decreases and thus vectorization is effective in both the transport and diffusion phases of the calculation.

III. References

1. R.D.O'Dell, F.W.Brinkley, D.R.Marr, R.E.Alcouffe, 'Revised User's Manual for ONEDANT: A Code Package for One-Dimensional, Diffusion-Accelerated, Neutral Particle Transport', Los Alamos National Laboratory, LA-9184-M, Rev. (1989)

Small FBR Benchmark Results

Reference discretization: 5 cm spatial mesh (14x14x30), S-8 (80 directions), 4 energy groups.

Calculational model: as in Fig. 2.

case 1. - control rod position filled with Na.

case 2. - control rod half inserted. $\Delta k = 1/k_2 - 1/k_1$

Integral results: (k_{eff}, Δk, iteration performance, computation time).

k_{eff}	case 1	case 2	Δk
S-4	0.973475	0.959361	0.01511
S-8	0.973479	0.959308	0.01517
S-12	0.973478	0.959299	0.01518
S-16	0.973477	0.959295	0.01519
(S-8)*	0.973600	0.959535	0.01506

Solution time: (YMP/8128 CPU seconds; () = XMP/24 CPU seconds)

	Trans sweeps		DSA solver		Total	
case	1	2	1	2	1	2
S-4	4.4	6.5	8.6	11.0	13.4 (16.1)	17.9 (22.0)
S-8	14.0	20.7	8.8	11.4	23.1 (25.7)	31.6 (35.4)
S-12	29.1	43.1	8.1	11.5	38.4	55.2
S-16	49.6	73.6	9.0	11.6	59.2	86.0
(S-8)*	27.4	44.3	16.1	21.3	44.4	66.7

Iteration performance: (number of iterations to 5e-5 convergence in S-8)

(S-8)	trans outers	trans inners	diff outers	diff inners
case 1.	7	29	19	958
case 2.	9	43	23	1231
(S-8)*				
case 1.	7	26	18	859
case 2.	8	42	21	1120

Computational performance: (for S-8 and (S-8)* solutions)

	trans sweep	diff sweep
T(μs) =	1.03	1.56
T* (μs)=	0.56	0.80

()* ⇒ 28x28x30 spatial mesh

LWR Benchmark Results

Reference discretization: 1 cm spatial mesh (25x25x25), S-8 (80 directions), 2 energy groups.

Calculational model: as in Fig. 1.

case 1. - control rod position empty.

case 2. - control rod in. $\Delta k = 1/k_2 - 1/k_1$

Integral results: (k_{eff}, Δk, iteration performance, computation time).

k_{eff}	case 1	case 2	Δk
S-4	0.976699	0.962355	0.01526
S-8	0.977144	0.962357	0.01572
S-12	0.977214	0.962308	0.01585
S-16	0.977232	0.962282	0.01590
(S-8)*	0.977194	0.962462	0.01566

Solution time: (YMP/8128 CPU seconds; () = XMP/24 CPU seconds)

	Trans sweeps		DSA solver		Total	
case	1	2	1	2	1	2
S-4	5.5	4.2	9.1	8.5	15.3 (18.2)	13.3 (15.8)
S-8	14.5	12.1	8.4	8.0	23.5 (27.9)	20.6 (23.7)
S-12	29.5	26.2	9.0	8.2	39.2	35.1
S-16	52.7	41.6	8.5	8.1	62.0	50.5
(S-8)*	50.4	34.4	25.3	17.5	77.8	53.6

Iteration performance: (number of iterations to 5e-5 convergence in S-8)

(S-8)	trans outers	trans inners	diff outers	diff inners
case 1.	7	18	16	462
case 2.	7	15	17	438
(S-8)*				
case 1.	8	25	17	-
case 2.	7	17	16	-

Computational performance: (for S-8 and (S-8)* solutions)

	trans sweep	diff sweep
T(μs) =	0.65	1.17
T* (μs) =	0.40	0.65

()* ⇒ 50x50x25 spatial mesh

Larger FBR Benchmark Results

Reference discretization: 5 cm spatial mesh (32x32x20), S-8 (80 directions), 4 energy groups.

Calculational model: as in Fig. 3.

case 1. - control rods inserted.

case 2. - control rods withdrawn. $\Delta k = 1/k_1 - 1/k_2$

case 3. - control rod positions filled with core material.

Integral results: (k_{eff}, Δk, iteration performance, computation time).

k_{eff}	case 1	case 2	Δk	case 3
S-4	0.970599	1.001289	0.03158	1.021841
S-8	0.969992	1.000797	0.03174	1.021418
S-12	0.969905	1.000727	0.03176	1.021340
S-16	0.969873	1.000704	0.03177	1.021331
(S-8)*	0.970347	1.000909	0.03147	-

Solution time: (YMP/8128 CPU seconds; () = XMP/24 CPU seconds)

	Trans sweeps			DSA solver			Total	
case	1	2	3	1	2	3	1	2
S-4	20.0	17.7	10.9	32.6	24.5	15.2	54.8 (60.9)	44.1 (55.3)
S-8	46.3	43.6	24.5	34.7	23.3	16.6	83.3 (94.4)	69.0 (77.8)
S-12	93.9	88.6	48.9	34.3	24.4	15.4	130.8	115.4
S-16	160.6	151.2	83.3	32.3	25.2	16.2	195.7	178.7
(S-8)*	123.0	108.5	-	67.4	63.3	-	194.8	175.9

Iteration performance: (number of iterations to 5e-5 convergence in S-8)

(S-8)	trans outers	trans inners	diff outers	diff inners
case 1.	10	53	41	2023
case 2.	8	50	24	1316
case 3.	6	28	20	968
(S-8)*				
case 1.	8	51	26	1400
case 2.	7	45	23	1354

Computational performance: (for S-8 and (S-8)* solutions)

	trans sweep	diff sweep
T(μs) =	0.53	0.84
T* (μs)=	0.37	0.59

()* ⇒ 64x64x20 spatial mesh

Keff Convergence as a Function of Number Sn Directions from the LWR Benchmark Problem.

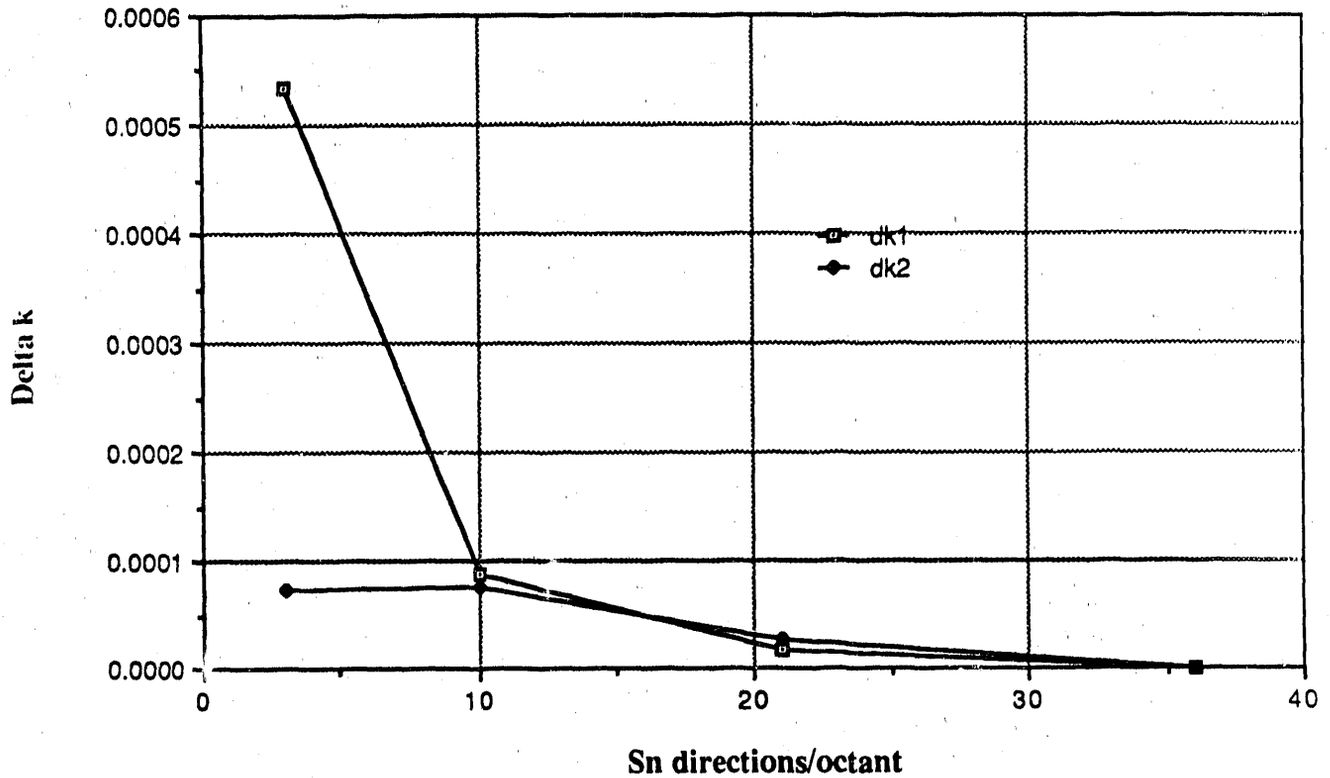

Keff Convergence as a Function of Number of Sn Directions from the Small FBR Benchmark Problem

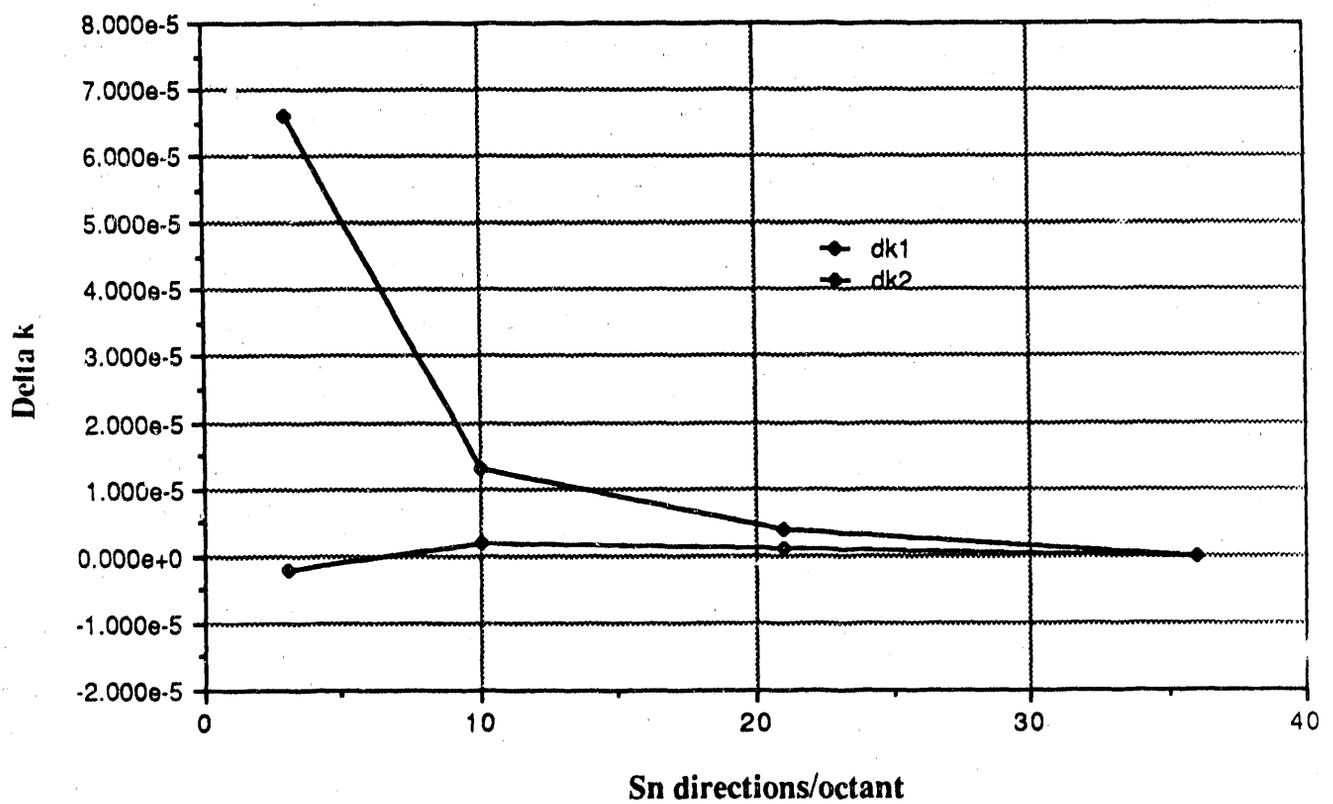

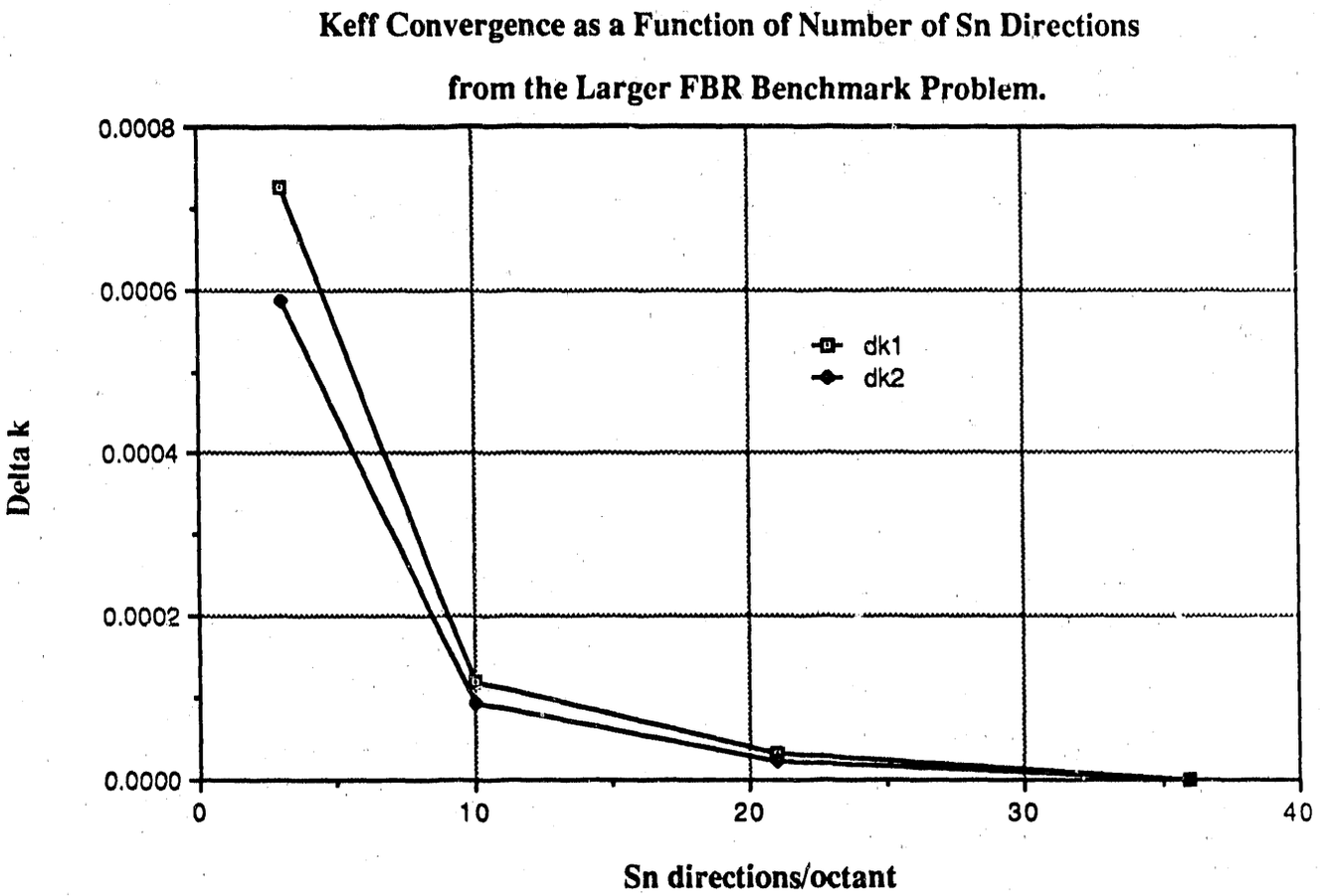
Keff Convergence as a Function of Number of Sn Directions
from the Larger FBR Benchmark Problem.
Delta k
0.0008
0.0006
0.0004
0.0002
0.0000
0
10
20
30
40
dk1
dk2
Sn directions/octant

Computation Times as a Function of Number of Sn Directions from the LWR Benchmark Problem.

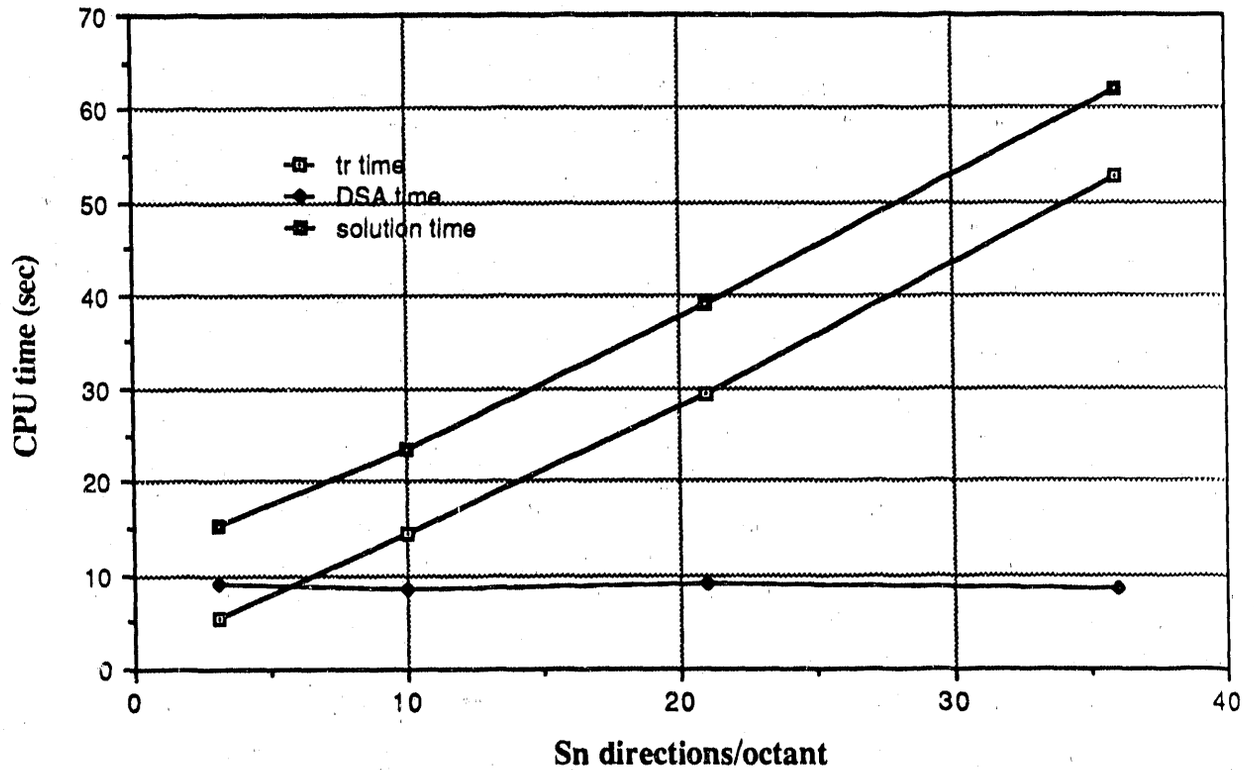

Computation Times as a Function of Number of Sn Directions from Larger FBR Benchmark Problem.

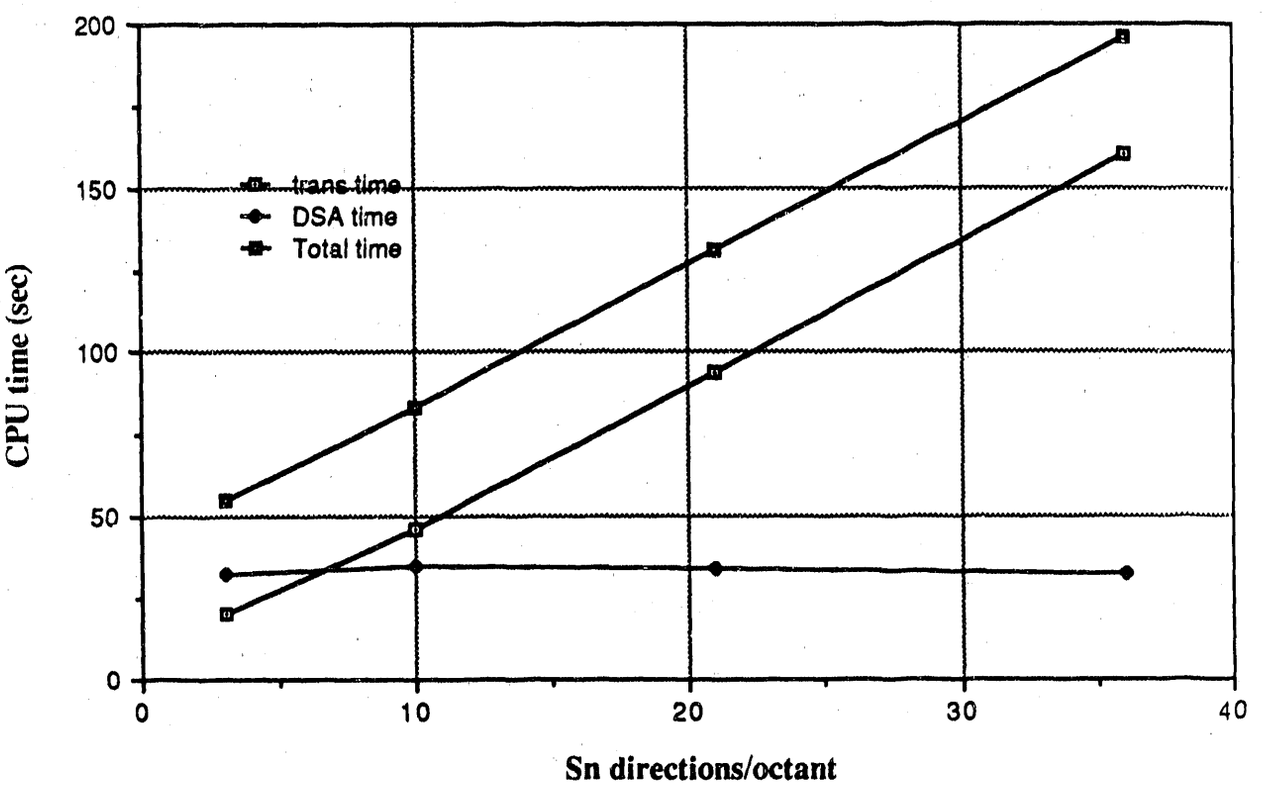

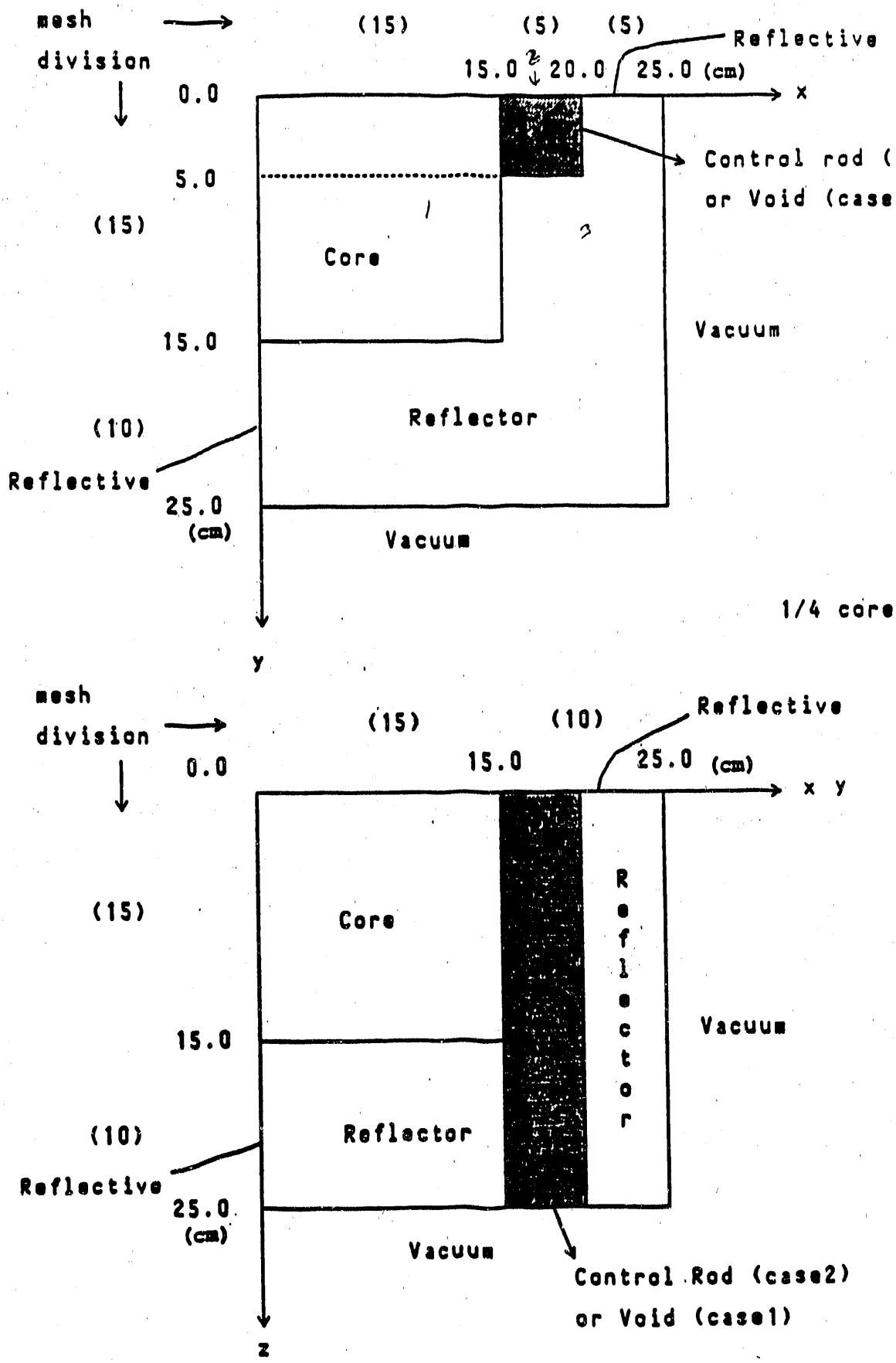

Fig. 1 Calculational model of Model 1 (small LWR)

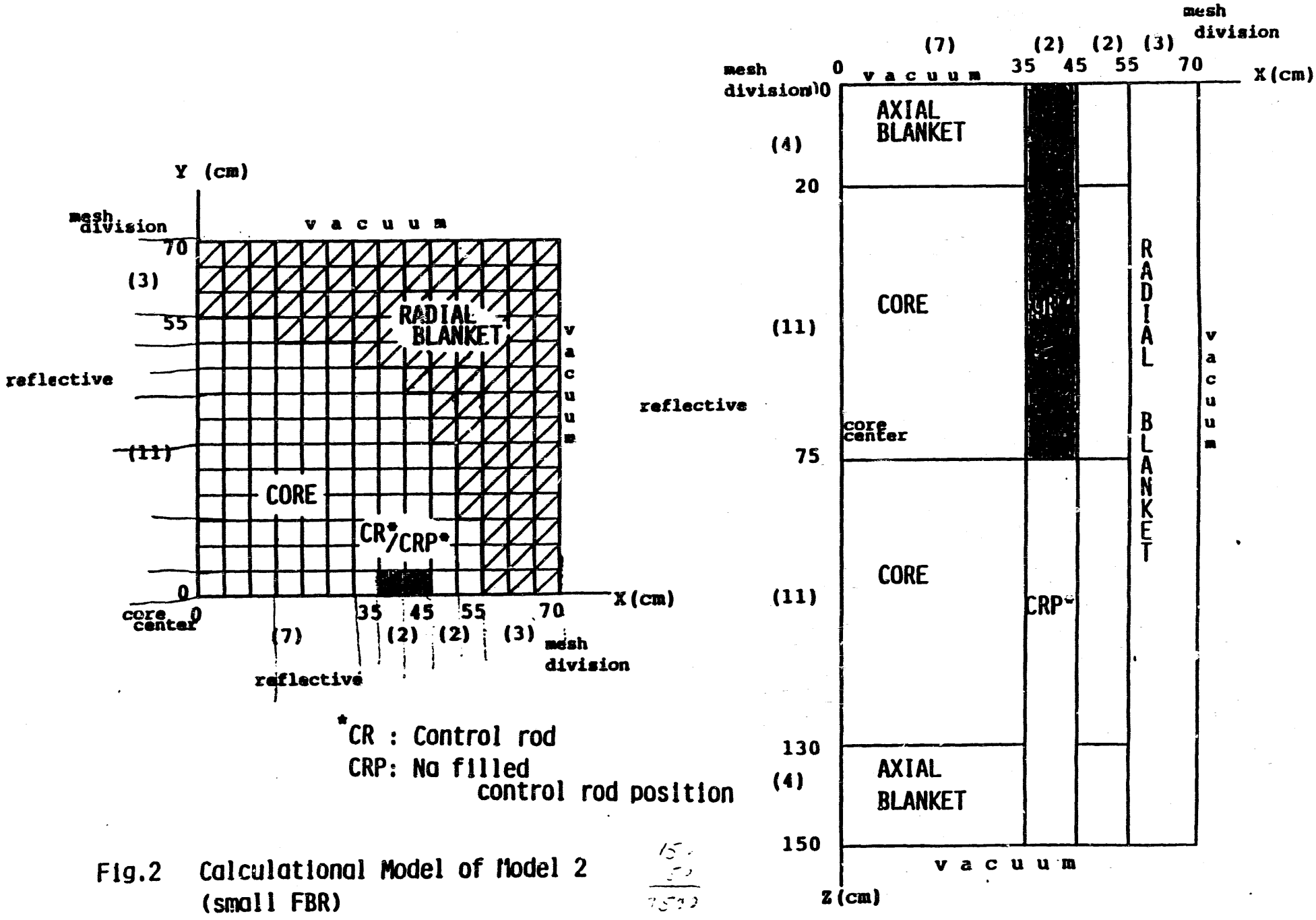

*CR : Control rod
CRP: Na filled control rod position

Fig.2 Calculational Model of Model 2 (small FBR)

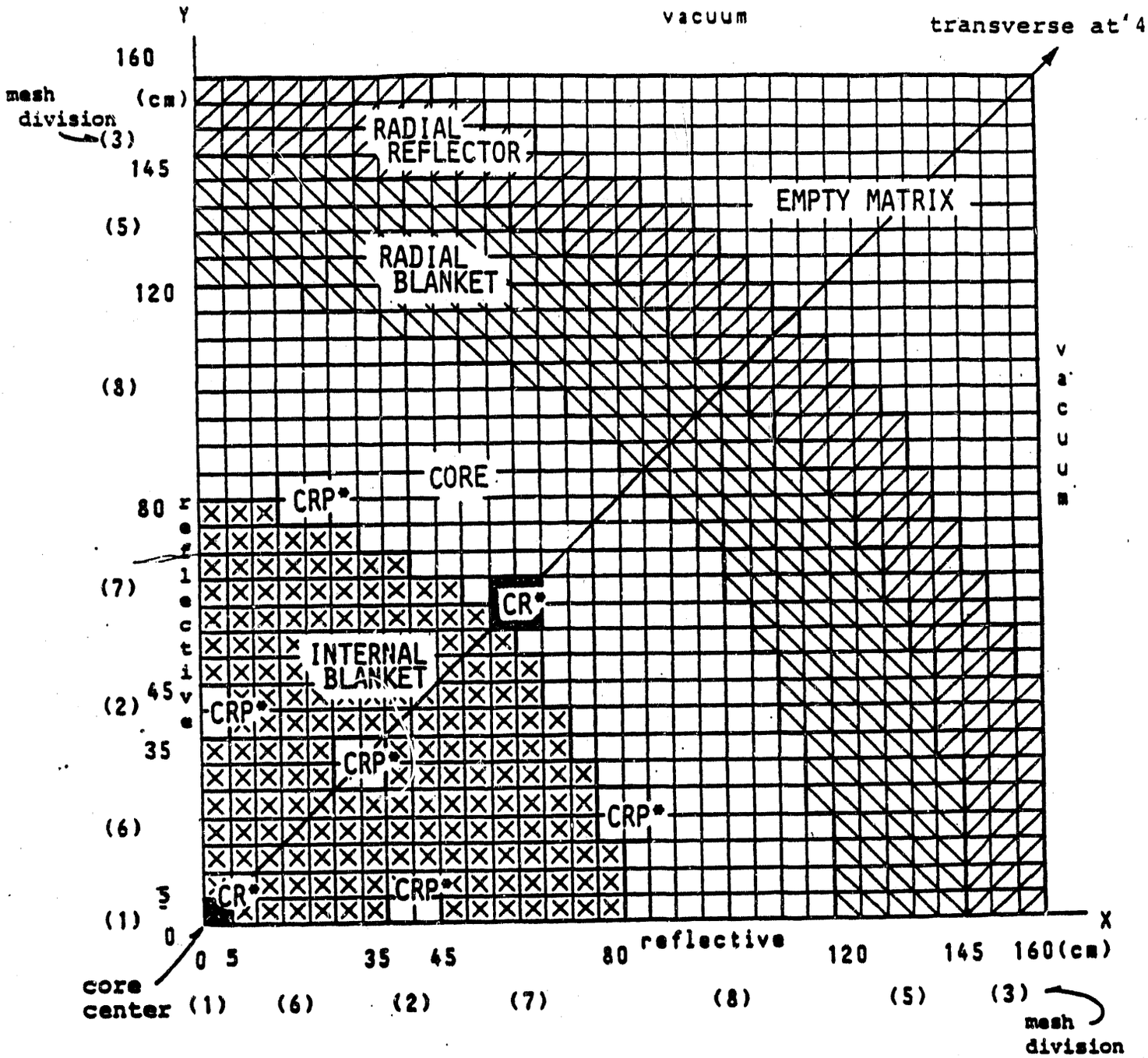

Fig. 3a XY cross sectional view of Model 3, Case 1 & 2 (axially heterogeneous FBR with control rod positions) at core midplane - 32 x 32 mesh, 1/4 core -

*CR : Control rod
CRP: Na filled control rod position

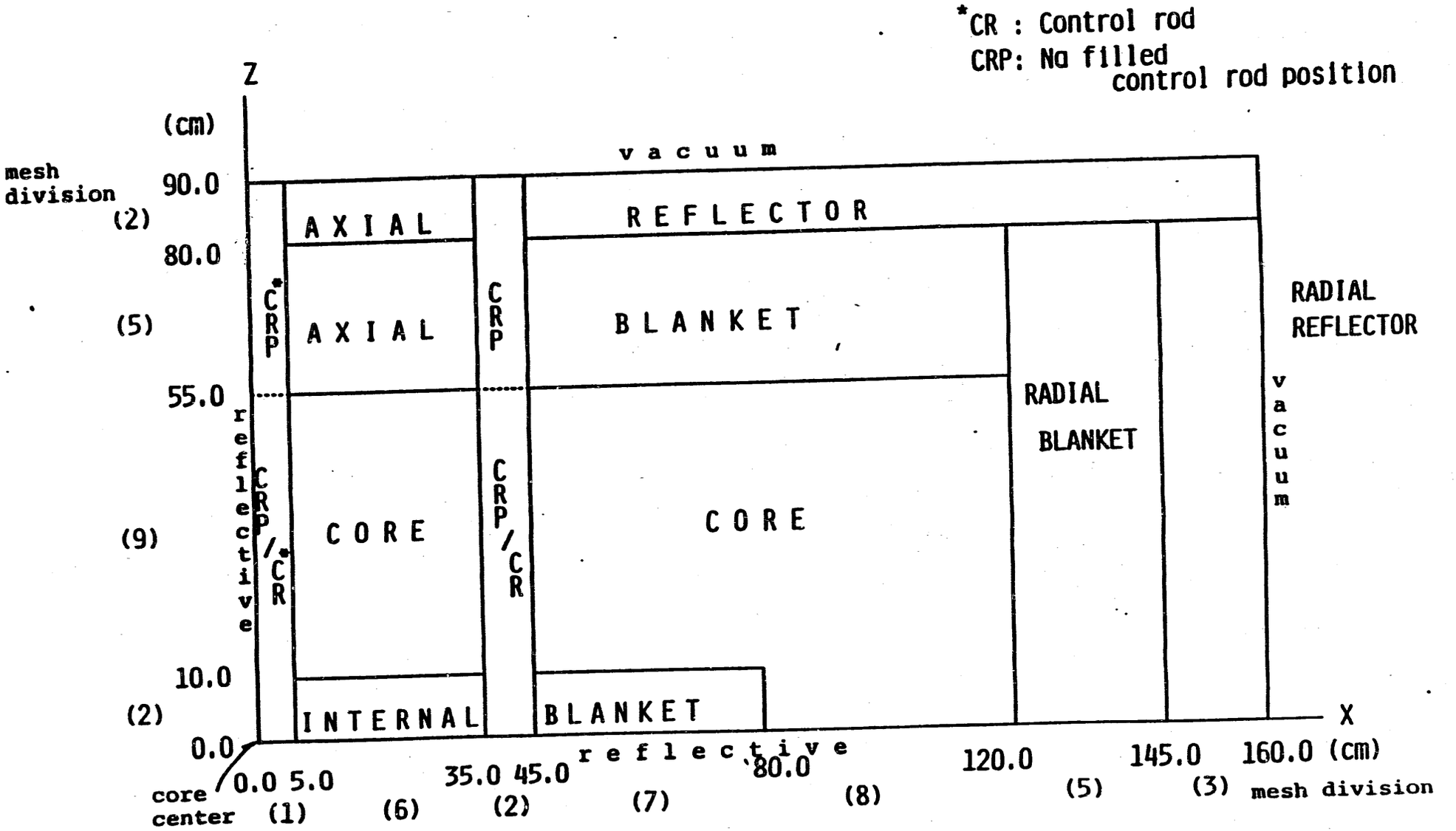

Fig. 3b XZ cross sectional view of Model 3, Case 1 & 2
(axially heterogeneous FBR with control rod positions)
at Y=0 plane

END

DATE FILMED

11 / 27 / 90